Importance of Partially Unfolded Conformations for Mg^{2+}-Induced Folding of RNA Tertiary Structure: Structural Models and Free Energies of Mg^{2+} Interactions†

Dan Grilley,[‡,§,||] Vinod Misra,[⊥] Gokhan Caliskan,[‡,@,#] and David E. Draper*[,‡,+]

Department of Biophysics, Program in Molecular and Computational Biophysics, and Department of Chemistry, Johns Hopkins University, Baltimore, Maryland 21218, Department of Pediatrics and Communicable Disease, University of Michigan, Ann Arbor, Michigan 48109, and Center for Neutron Research, National Institute of Standards and Technology, Gaithersburg, Maryland 20899

Received November 4, 2006; Revised Manuscript Received April 20, 2007

ABSTRACT: RNA molecules in monovalent salt solutions generally adopt a set of partially folded conformations containing only secondary structure, the intermediate or I state. Addition of Mg^{2+} strongly stabilizes the native tertiary structure (N state) relative to the I state. In this paper, a combination of experimental and computational approaches is used to estimate the free energy of the interaction of Mg^{2+} with partially folded I state RNAs and to consider the possibility that Mg^{2+} favors "compaction" of the I state to a set of conformations with a higher average charge density. A sequence variant with a drastically destabilized tertiary structure was used as a mimic of I state RNA; as measured by small-angle X-ray scattering, it adopted a progressively more compact conformation over a wide Mg^{2+} concentration range. Average free energies of the interaction of Mg^{2+} with the I state mimic were obtained by a fluorescence titration method. To interpret these experimental data further, we generated molecular models of the I state and used them in calculations with the nonlinear Poisson−Boltzmann equation to estimate the change in Mg^{2+}−RNA interaction free energy as the average I state dimensions decrease from expanded to compact. The same models were also used to reproduce quantitatively the experimental difference in excess Mg^{2+} between N and I states. On the basis of these experiments and calculations, I state compaction appears to enhance Mg^{2+}−I state interaction free energies by 10−20%, but this enhancement is at most 5% of the overall Mg^{2+}-associated stabilization free energy for this rRNA fragment.

The folding of a RNA tertiary structure has been described as an equilibrium between partially folded molecules with only secondary structure, sometimes called an I (intermediate) state, and the fully folded native conformation, or N state (*1*, *2*). RNA tertiary structures tend to be strongly stabilized by low concentrations of Mg^{2+} ion (*3*, *4*), which implies that the N state interacts more favorably with Mg^{2+} than does the I state (*5*). The origins and magnitude of this difference in interaction free energies have been the subject of experimental and theoretical work for a number of years. Much of the effort has been concerned with establishing a physical basis for strong interactions of ions with folded RNAs (*6*−*8*). Interactions of ions with the I state have not received as much attention, though early work with transfer RNA (analyzed in ref *9*) and recent studies of two other RNAs (*10*, *11*) have found relatively strong interactions of Mg^{2+} with partially unfolded forms of these RNAs, and suggest that I state RNA properties will have to be considered in any quantitative description of the effects of Mg^{2+} on RNA stability.

As part of our effort to understand the energetics of Mg^{2+}-induced RNA tertiary folding (*9*, *10*), in this paper we focus on the free energy of interactions of Mg^{2+} with the partially unfolded states of a RNA. In considering these interactions, it is important to note that the I state is potentially a broad distribution of many different conformations with similar energies, and the average properties of this ensemble may be sensitive to the mono- and divalent salt concentrations present in solution. It has long been known that the dimensions of a flexible linear polyelectrolyte (e.g., carboxymethylcellulose) can be reduced by added salt to nearly those of the uncharged form of the polymer (*12*). Though the secondary structure of an I state RNA reduces its number of conformational degrees of freedom compared to that of an unstructured polymer, it is nevertheless likely that the average dimensions of partially unfolded RNA will be sensitive to added salt to some degree.

† This work was supported by NIH Grant 1RO1 GM58545. G.C. received support from the National Institute of Standards and Technology (to Dr. R. Briber). Use of the Advanced Photon Source was supported by the U.S. Department of Energy under Contract W-31-109-ENG-38. BioCAT is a Research Center supported by the National Institutes of Health (RR-08630).

‡ Department of Biophysics, Johns Hopkins University.

§ Program in Molecular and Computational Biophysics, Johns Hopkins University.

|| Present address: Department of Biochemistry, Molecular Biology and Cell Biology, Northwestern University, Hogan Biological Sciences Building, 2205 Tech Dr., Evanston, IL 60208-3500.

⊥ University of Michigan.

@ National Institute of Standards and Technology.

Present address: National Organik Adhesives Ltd., Cendere Yolu No 16, Ayazaga Istanbul 34396, Turkey.

+ Department of Chemistry, Johns Hopkins University.

[1] Abbreviations: R_g, radius of gyration; HQS, 8-hydroxyquinoline-5-sulfonic acid; SAXS, small-angle X-ray scattering; NLPB, nonlinear Poisson−Boltzmann.

10.1021/bi062284r CCC: $37.00
Published on Web 08/18/2007

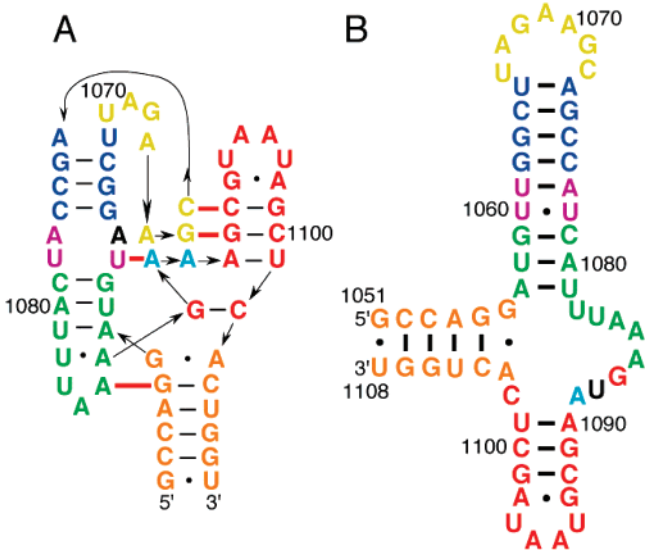

FIGURE 1: Variants of the 58-nucleotide fragment of large subunit ribosomal RNA from *E. coli* (nucleotides 1051−1108) used in this study. Mutations from the *E. coli* sequence are colored black. (A) U1061A RNA drawn to indicate base pairs (black horizontal lines) and tertiary base−base hydrogen bonding (red bars) in the folded RNA (*14*). Arrows indicate the 5′ to 3′ direction of the backbone. (B) A1088U RNA, in which the A1088−U1060 tertiary interaction has been disrupted, drawn with the secondary structure used in modeling of I state conformations (see the text).

The equilibrium folding of a RNA tertiary structure in response to added Mg^{2+} might therefore be conceptualized as consisting of two steps: formation of a compact I state intermediate, followed by formation of tertiary contacts that stabilize the N state. In such a scheme, two extreme scenarios could be imagined with regard to how Mg^{2+} stabilizes the native state. It has been suggested that compact, Mg^{2+}-dependent RNA conformations are common equilibrium folding intermediates from which conformational searches for sets of tertiary interactions take place (*13*). In this scenario, Mg^{2+} stabilization of a compact RNA ensemble pays for much of the overall thermodynamic cost of overcoming the electrostatic and entropic barriers to folding. Alternatively, if Mg^{2+} affected the distribution of I state conformations to only a small degree, most of the stabilization energy would come from strong interactions of Mg^{2+} with the folded N state. To evaluate these two potential roles for Mg^{2+} in the folding of a RNA, here we explore how the strength of Mg^{2+}−RNA interactions varies with compaction of the I state ensemble and compare those free energies to those of interactions of Mg^{2+} with the native state.

The RNA studied in this paper is a 58-nucleotide fragment of rRNA, diagrammed in Figure 1. It folds into a very compact structure stabilized by noncanonical hydrogen bonding between bases (red bars in Figure 1A) and a number of other tertiary interactions (*14*). The three-helix junction in the partially unfolded form of this RNA (Figure 1B) has the potential to adopt either extended or compact conformations. We use a combination of experimental and computational approaches to evaluate changes taking place in the average properties of the I state as Mg^{2+} is added to a RNA and estimate the increases in Mg^{2+}−RNA interaction free energies as the I state becomes progressively more compact. Our analyses of interaction of Mg^{2+} with the I state structural models developed in this work complement a previous quantitative model for interactions of Mg^{2+} ion with the N state of the same RNA (*6*). Together, these models provide the most comprehensive view yet developed for the equilibrium means by which Mg^{2+} ions stabilize a native RNA tertiary structure.

MATERIALS AND METHODS

Materials and Buffers. All buffers and salts were purchased as reagents of at least 99.5% purity. High-quality water (18 MΩ resistivity) was used throughout. 8-Hydroxyquinoline-5-sulfonic acid (HQS)[1] was purchased from Sigma and purified as described previously (*5*). The standard buffer for RNA experiments contained 20 mM MOPS or MES, adjusted to the desired pH with KOH, 20 μM EDTA, and various concentrations of KCl. The total K^+ concentration (from the pH-adjusted buffer and added KCl) is specified for all the experiments.

Nucleic Acid Preparations. Two 58-nucleotide RNAs were transcribed from plasmid DNA. The sequences are variants of nucleotides 1051−1108 of the *Escherichia coli* 23S rRNA, U1061A or A1088U (*15*). RNAs were prepared by runoff transcription from plasmids linearized with RsaI endonuclease using the following conditions (*16*): 200 mM HEPES (pH 7.5), 28 mM $MgCl_2$, 40 mM DTT, ATP, CTP, GTP, and UTP (6 mM each), 2% PEG-8000, 40 μg/mL linearized template DNA, and an optimized concentration of T7 RNA polymerase modified with a His6 tag and purified as described previously (*17*). Transcripts were purified under denaturing conditions using a DEAE column matrix from Qiagen, as described previously (*5*), and appeared at least 95% pure when run on denaturing polyacrylamide gels.

Double-stranded DNA was prepared from plasmid pUC18 purified by density gradient centrifugation in CsCl. To reduce the solution viscosity for titrations with $MgCl_2$, the plasmid was first digested with BanI, HhaI, and NlaIII endonucleases at 37 °C, heated to 65 °C, and digested with Taq αI (New England Biolabs). The digested DNA was purified over a DEAE column as described previously (*5*) to remove small restriction fragments and proteins. This procedure produced DNA fragments ranging in size from ∼75 to 200 bp.

RNA Folding Monitored by UV Absorbance. The U1061A rRNA fragment studied here adopts a compact conformation with an extensive set of tertiary contacts, as seen in a crystal structures of the RNA bound to a ribosomal protein domain, L11−C76, normally associated with the RNA domain in the ribosome (*14*). Hydroxyl radical footprinting experiments indicate that the same set of tertiary contacts is formed in the presence or absence of the protein, if Mg^{2+} ion is present (*18*). In melting experiments with U1061A RNA, Mg^{2+} induces the appearance of a new unfolding transition with distinctive optical properties, viz., hyperchromicity at 260 nm, virtually no absorbance change at 280 nm, and ∼20% hypochromicity at 295 nm (Figure S1 of the Supporting Information). We identify this structural transition with disruption of tertiary structure for two reasons, in addition to its Mg^{2+} dependence: it is strongly coupled to L11−C76 binding (*19*, *20*), and the stability of the structure depends on the monovalent ion type in a way that is consistent with the observation of a chelated K^+ ion within the tertiary fold (*18*, *21*). Because no other structural transitions in this RNA are associated with changes in absorbance at 295 nm, we

monitor this wavelength as an assay of tertiary structure formation.

RNA absorbance versus temperature profiles (melting curves) were measured at 260, 280, and 295 nm with a Cary Bio400 spectrophotometer. Both heating and cooling curves were obtained, to check the reversibility of the transitions. The temperature was ramped at a rate of ±0.6 °C/min. Experiments determining the extent of RNA folding during isothermal titration with $MgCl_2$ were carried out in the same spectrophotometer equipped with a computer-controlled Hamilton syringe, by described methods (*10*). These melting and titration experiments were used to determined appropriate solution conditions for carrying out measurements of Mg^{2+}−RNA interactions (next section). At the lowest monovalent cation concentration that was used, 20 mM K^+, 15 °C was below the onset of any unfolding transitions observed in melting profiles of A1088U and U1061A RNAs in the absence of Mg^{2+} (Figure S2 of the Supporting Information). Titration of U1061A RNA with Mg^{2+} under the same solution conditions showed that 260 and 295 nm monitored the same tertiary folding transition, but in a similar titration at 25 °C, folding of secondary structure (monitored at 260, 270, and 280 nm) preceded tertiary folding as assayed at 295 nm (Figure S3 of the Supporting Information). Therefore, 15 °C was chosen for the Mg^{2+}−RNA titrations described below, to ensure that titration with $MgCl_2$ did not induce additional secondary structure in A1088U RNA and that U1061A RNA folded in a single, two-state transition.

UV-monitored titrations of U1061A RNA were used to find the fraction of RNA folded (and thus the free energy of folding, $\Delta G^\circ_{obs,2+}$) as a function of the Mg^{2+} concentration, as described previously (*10*). The Wyman linkage relation, as derived for Mg^{2+} interacting with RNA under conditions of constant excess KCl (*10*)

$$\left(\frac{1}{RT}\right)\left(\frac{\partial \Delta G^\circ_{obs,2+}}{\partial \ln C_{2+}}\right) \cong \Gamma^N_{2+} - \Gamma^I_{2+} = \Delta\Gamma_{2+} \qquad (1)$$

was then used to calculate the difference in the excess Mg^{2+} ($\Delta\Gamma_{2+}$, defined below in eq 3) between the folded and partially folded states of the RNA.

Fluorescence Measurements of Mg^{2+}−RNA Interactions. A method for assessing the interactions between Mg^{2+} ions and a RNA and an interpretation of the experimental data in terms of thermodynamic quantities have been described in detail (*5*, *10*). In brief, the approach takes advantage of a fluorescent dye, HQS, in detecting the effective concentration of Mg^{2+} ion in the presence of RNA. Data are collected from an Aviv ATF105 fluorimeter equipped with computer-controlled Hamilton syringes. Two cuvettes are prepared with identical concentrations of buffer and dye; RNA equilibrated with the same buffer is added to the sample cuvette. Titration of buffer containing $MgCl_2$ into both cuvettes results in enhanced fluorescence from the dye. More $MgCl_2$ must be added to the sample cuvette to reach the same level of fluorescence seen in the reference cuvette lacking RNA, because interactions between Mg^{2+} ions and the RNA lower the Mg^{2+} activity. When sample and reference cuvettes have identical fluorescence intensities, the "excess" Mg^{2+} per RNA, ΔC^{RNA}_{2+}, is defined as

$$\Delta C^{RNA}_{2+} = \frac{C_{2+,sample} - C_{2+,ref}}{C_{RNA}} \qquad (2)$$

where $C_{2+,sample}$ and $C_{2+,ref}$ are the molar concentrations of Mg^{2+} in the sample and reference cuvettes, respectively, and C_{RNA} is the concentration of RNA molecules. $C_{2+,ref}$ is the "bulk" Mg^{2+} ion concentration; we refer to this quantity using the shorthand notation C_{2+}.

Titrations at different K^+ concentrations were carried out at different pHs, to optimize the sensitivity of the experiment to measurements in different ranges of C_{2+} by adjusting the affinity of HQS for Mg^{2+}. The pHs and buffers used were as follows: pH 7.2 with MOPS, pH 7.0 with MOPS, pH 6.8 with MOPS, and pH 6.15 with MES. The stability of the RNA tertiary structure studied here is not pH-dependent in this range (unpublished observations). In general, a higher pH was used at lower K^+ concentrations. Titrations carried out at different pHs but the same K^+ concentration gave consistent results.

ΔC^{RNA}_{2+} approaches the thermodynamic quantity Γ_{2+} when there is an at least 30-fold excess of KCl over $MgCl_2$, the solutions are sufficiently dilute that molar and molal concentration units are interchangeable, and ΔC^{RNA}_{2+} is independent of RNA concentration (*10*); all of these conditions apply to the experiments reported here. For the four-component system used in these studies (water, K^+ salt of RNA, KCl, and $MgCl_2$), Γ_{2+} is defined as

$$\Gamma_{2+} \equiv \left(\frac{\partial m_{2+}}{\partial m_{RNA}}\right)_{T,P,\mu_4,m_3} \qquad (3)$$

where the temperature (T), pressure (P), $MgCl_2$ chemical potential (μ_4), and KCl molality (m_3) are held constant. m_{2+} is the Mg^{2+} molality, and m_{RNA} is the RNA molality. m_{2+} approaches the bulk Mg^{2+} concentration as the RNA becomes infinitely dilute and is equivalent to C_{2+} under the limiting experimental conditions used here. Γ_{2+} is also obtained from the electrostatic calculations described below; thus, the experimental and theoretical results can be directly compared. A more detailed discussion of Γ_{2+} and its relation to ΔC^{RNA}_{2+} appears in ref *10*.

Free energies of Mg^{2+}−RNA interactions were obtained by integration of plots of ΔC^{RNA}_{2+} as a function of $\ln(C_{2+})$ (*10*)

$$\Delta G_{RNA-2+} \cong -RT \int_0^{C_{2+}} \Delta C^{RNA}_{2+}\, d[\ln(C_{2+})] \qquad (4)$$

This equation is applicable only to dilute solutions with an excess of KCl over $MgCl_2$, as mentioned above. Integrals were obtained from fits of the data to a polynomial which asymptotically approaches the abscissa at low values of $\ln(C_{2+})$, $y = b(x - a)^2 + c(x - a)^3 + d(x - a)^4$.

Small-Angle X-ray Scattering Measurements. Small-angle X-ray scattering (SAXS) experiments were performed on the Biocat 1D18 beamline at the Argonne National Laboratory's Advanced Photon Source for both the U1061A and A1088U RNAs. Measurement of the scattering intensity was performed for RNA samples pre-equilibrated in 20, 40, 60, and 150 mM K^+ buffers and 40 mM K^+ buffer with 0.01, 0.1, 1.0, and 10 mM bulk Mg^{2+}. GNOM (*22*) was used to calculate the radius of gyration from the SAXS intensities;

intensities with momentum transfers between 0.017 and 0.2 $Å^{-1}$ were used in the calculations. The parameters for the upper and lower bounds, the baselines, and the weighting function were varied. All of the R_g values from estimated fits with a score of ≥ 0.75 were used to compute the reported average and standard deviation.

Molecular Modeling. Molecular models of possible I state conformations were generated using XPLOR-NIH (*23*), starting from randomized backbone conformations and distance and angle constraints chosen to maintain base pairing in selected parts of the RNA. Previous NMR studies of fragments of the 58mer RNA (*24*−*26*) and thermal denaturation of the RNA and its fragments (*27*) have defined helical segments likely to be present in the I state. There is some uncertainty about U1082-A1086 and G1087-C1102 base pairs (Figure 1A), which are unlikely to remain paired in the absence of tertiary interactions and have the potential to mispair with other bases in the junction loop. Mfold (*28*) was used to calculate the free energies of the most likely alternatives, and on that basis, distance and angle constraints were chosen to be consistent with the secondary structure shown in Figure 1B.

A1088U RNA sequences with randomized backbone and χ angles were used as a starting point for generating models in XPLOR-NIH. Ideal bond distances and angles, atomic radii, and improper angles were taken from the parnah1er1_mod_new.inp parameter file included with XPLOR-NIH. Synthetic distance and torsion angle constraints were created to maintain nucleotides in the helical segments in an A-form conformation. Distances and geometries for standard Watson−Crick residues were obtained from ideal A-form RNA helices output by the Insight II software package (Biosym). Noncanonical base pair and hairpin loop constraints were obtained from analysis of the 58-nucleotide RNA/L11−C76 cocrystal structure (PDB entry 1HC8) or from NMR constraints for a hairpin similar to the helix of nucleotides 1057−1081 (*24*). Hydrogen−hydrogen distances of less than 5 Å in the base-paired helices were used in creating the constraints. The range allowed for each distance was at most 20% of the measured distance, with tighter constraints used for hydrogen bond constraints. Intranucleotide distances for residues at the end of a helix were eliminated to allow the terminal base pairs additional flexibility. Because they frequently resulted in the rejection of structures that would otherwise satisfy all other constraints, distances involving either the 2′-OH group or stereospecific hydrogens were also eliminated. In addition, backbone and χ torsion angles obtained from the models described above were constrained to the following ranges: $\pm 10°$ for residues in canonical A-form helices, $\pm 20°$ for residues in hairpin loops, and $\pm 30°$ for the α and β angles of U1060 (based on the NMR constraints). The α, β, and γ angles or the ϵ and ζ angles were unconstrained for residues at the 3′ or 5′ ends of helices, respectively. These constraints, coupled with the high weights put on them, were designed to force the formation of helices without biasing their arrangement.

The final structures were generated by a restrained molecular dynamics protocol. As the only goal was the creation of sterically allowed structures, only bond lengths, bond angles, and van der Waals interactions were specified in addition to the constraints detailed above. The protocol was as follows. First, 16 000 minimally constrained dynamics steps in Cartesian space at 1600 K were carried out, followed by 8000 steps with the NOE, improper, and bond angle weights increased. The system was then slowly cooled in 50 K steps to 100 K while the Van der Waals radii were reduced and the level of steric repulsion was increased. The final step was a minimization with the weights for all of the constraints set to 1. Of the 617 total structures, 480 were rejected for angles and distances deviating from the initial constraints by specified criteria. Eight additional structures were rejected because they contained topological knots, leaving 129 models.

For comparison with experimental measurements of U1088A RNA, the R_g of the calculated models was computed using CRYSOL (*29*) which calculates the scattering from an atomic-resolution structure and a first hydration layer around the macromolecule. No allowance is made for accumulation of ions near the RNA surface.

To determine the range of conformations adopted by the junction, angles were calculated between vectors normal to the C1052-G1107, U1058-A1080, and C1091-G1100 base pairs. The vectors normal to the base pairs were calculated with 3DNA (*30*). There were no significant correlations between any two pairs of angles (not shown).

Calculations with the NLPB Equation. Finite difference solutions to the nonlinear Poisson−Boltzmann (NLPB) equation for our RNA structural models in various ion solutions were obtained using Qnifft (*31*, *32*). This program maps the surface of the RNA onto a $65 \times 65 \times 65$ grid. The RNA was treated as a low-dielectric medium (ϵ_m) within a volume enclosed by its water-accessible surface (probe radius = 1.4 Å). Results are presented for an ϵ_m of 2, a physically reasonable value that accounts for the effects of electronic polarizability (*33*, *34*). The cvff91 parameter set for the nucleic acid was used to define the atomic charges and sizes. The surrounding solvent was treated as a continuum with a uniform dielectric constant (ϵ_s) of 80. The surrounding K^+, Mg^{2+}, and Cl^- were distributed according to a Boltzmann weighted average of the mean electrostatic potential. A 2.0 Å ion exclusion radius was added to the surface of the macromolecule to account for ion size. Addition of protons and fixed ions to the native structure (PDB entry 1HC8) was carried out as described previously (*6*).

A two-step focusing procedure was used to calculate the potentials around the RNA. The RNA was initially mapped onto a grid of ~0.1 grid/Å and the NLPB equation solved with the boundary condition that the potentials are zero at the edge of the grid. The RNA was then mapped onto a higher-resolution grid with the boundary potentials taken from the results of the initial grid; the grid spacings were chosen so that the boundary of the new grid mapped exactly onto a set of lattice points from the initial grid. This procedure was repeated a third time with a final resolution between 0.65 and 1.2 grids/Å (I state) or between 1.0 and 1.2 grids/Å (N state), chosen so that charge neutrality was maintained within 2%. The relevant integrals for calculating the K^+- and Mg^{2+}-dependent contributions to RNA stability were evaluated as a summation over discrete lattice points as described previously (*35*, *36*). In each case, the ion atmosphere was integrated over the lattice generated in the two focusing runs and summed together. Electrostatic potentials were iterated to a convergence of less than 10^{-4}

kT/e. The results presented here varied by less than 1% for focusing procedures where charge neutrality was maintained within 2%.

BACKGROUND

The conformations composing the I state ensemble of a RNA potentially undergo a continuous shift to more compact dimensions as Mg^{2+} concentrations increase. The object of this study is to compare the free energy contributed by Mg^{2+} to the stabilization of compact RNA conformations with the additional stabilization free energy Mg^{2+} affords the N state. To incorporate a compaction free energy into a thermodynamic framework for Mg^{2+}-dependent RNA folding, we first define two different ensembles of I state RNA conformations which represent limits for computing changes in Mg^{2+}−I state interaction free energies. I_E is the set of expanded conformations present at a particular temperature and K^+ concentration in the absence of Mg^{2+}, and I_C is the ensemble of compact conformations from which the tertiary structure folds at a specific bulk Mg^{2+} concentration (C_{2+}). As a convenient point for comparing compaction and folding stabilization free energies, we define I_C as the ensemble present at the midpoint of the folding transition, where the Mg^{2+} concentration is C^0_{2+} and the I_C and N states are equally represented.

Γ_{2+} is a thermodynamic function, the "excess" Mg^{2+} per RNA (Materials and Methods, eq 3), which represents the interactions taking place between all Mg^{2+} ions in solution and a RNA. Extremes in the possible Mg^{2+} dependence of Γ_{2+} for the defined ensembles are presented in panels A and B of Figure 2. Γ_{2+} curves for the I_E ($C_{2+} = 0$) and I_C ($C_{2+} = C^0_{2+}$) ensembles (solid lines) are drawn as if the distribution of conformations in each ensemble remains fixed in the defined state. Because the RNA undergoes a shift from the I_E to I_C ensembles with the addition of Mg^{2+}, the observed values of Γ_{2+} of the I state ensemble (red dashed line) should lie between Γ_{2+} for the two defined ensembles. For a native sequence RNA, the N state appears as the dominant RNA conformation as the Mg^{2+} concentration approaches C^0_{2+} and Γ_{2+} increases further (dashed blue line). Compaction of the RNA I state could be associated with small (Figure 2A) or large (Figure 2B) changes in Γ_{2+}, compared to the increase in Γ_{2+} taking place in the folding reaction.

The relative free energies of the three RNA ensembles (I_E, I_C, and N states) are defined in the thermodynamic cycles of Figure 2C. The vertical arrows represent transitions between extended (I_E), compact (I_C), and native (N) conformations, in the presence (right side of the cycle) or absence (left side of the cycle) of a given Mg^{2+} concentration (at a constant concentration of K^+). The horizontal arrows define the free energies of interaction of Mg^{2+} with the I_E, I_C, and N state ensembles of RNA conformations. The free energy contributed by Mg^{2+} toward compaction of the RNA is the difference between free energies associated with either the vertical or horizontal arrows

$$\Delta\Delta G_{comp,2+} = \Delta G^\circ_{comp,2+} - \Delta G^\circ_{comp,0} = \Delta G_{I_C-2+} - \Delta G_{I_E-2+} \quad (5)$$

A similar set of equations applies to the Mg^{2+}-dependent stabilization of N over the I_C state, $\Delta\Delta G_{fold,2+}$, using the free energies defined in the bottom half of the cycle (*10*). (We emphasize again that I_E and I_C are defined as fixed ensembles of conformations, independent of Mg^{2+} concentrations. Though some states represented in the thermodynamic cycle cannot be experimentally observed, I_C in the absence of Mg^{2+}, for instance, they are necessary for using computational means to parse experimental data into separate Mg^{2+} interaction and folding free energies.)

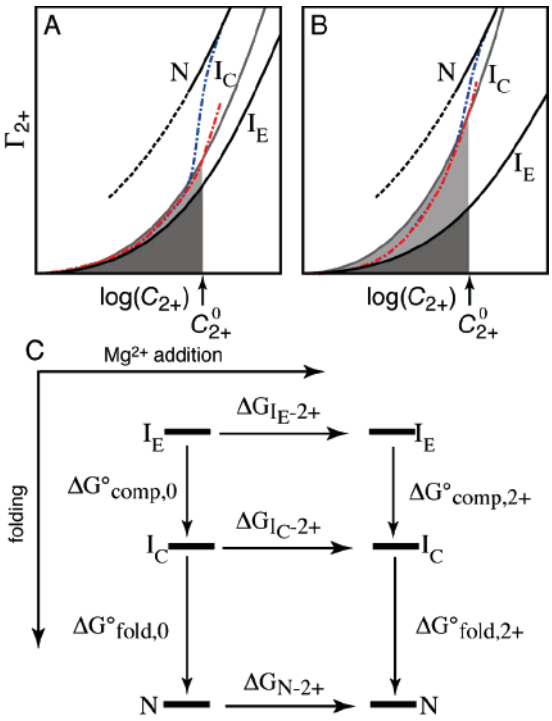

FIGURE 2: Thermodynamics of interactions of Mg^{2+} ion with folded and partially unfolded states of a RNA. (A and B) Relation between Γ_{2+} and Mg^{2+}−RNA interaction free energies for hypothetical cases in which compaction of the RNA I state plays a minor (A) or major (B) role in the Mg^{2+}-dependent folding energetics. Hypothetical Γ_{2+} curves are shown for expanded and compact folded states (I_E and I_C, respectively) and the native (N) state of a RNA. The behavior of Γ_{2+} for the N state at C_{2+} below the folding transition is unknown. The dashed red lines represent the Γ_{2+} curve that might be experimentally observed for a RNA unable to fold to the native state. The dashed blue lines are the observed Γ_{2+} curves for a RNA that folds to the native state. Shaded areas are proportional to free energies of interaction of Mg^{2+} with different RNA states (eq 4): the dark gray area corresponds to $-\Delta G_{I_E-2+}/RT$, and the light gray area is the difference $\Delta\Delta G_{comp,2+}/RT = -(\Delta G_{I_C-2+} - \Delta G_{I_E-2+})/RT$ (free energies are defined in panel C). (C) Thermodynamic cycle for Mg^{2+}-induced RNA folding by the equilibrium pathway $I_E \rightarrow I_C \rightarrow N$. The upper square describes RNA compaction and the lower square tertiary structure folding. Vertical arrows are standard state free energies for equilibria between the different RNA forms in the presence (right) or absence (left) of Mg^{2+} ion. Horizontal arrows are the free energies of interactions of Mg^{2+} with each of the three RNA states.

The free energies of interaction of Mg^{2+} with the I_E and I_C ensembles are proportional to the areas under the Γ_{2+} versus log(C_{2+}) curves in panels A and B of Figure 2 (Materials and Methods, eq 4). Thus, $\Delta\Delta G_{comp,2+}$ is represented by the gray areas between the I_E and I_C state curves in panels A and B. In the extreme case in which there is a large degree of I state compaction (Figure 2B), much of the overall work done by Mg^{2+} in stabilizing the native fold occurs in compaction of the RNA.

In this study, we use two strategies to resolve the experimentally observed Γ_{2+} curve for a RNA into individual Γ_{2+} curves for the I_E and I_C structural ensembles. First, we analyze interactions of Mg^{2+} with the variant A1088U RNA as a mimic of the I state. This RNA has a mutation in a key tertiary Hoogsteen base pair and consequently does not exhibit any evidence of a tertiary unfolding transition in melting experiments carried out at K^+ and Mg^{2+} concentrations used in the experiments reported here (ref *37* and data not shown). This RNA can therefore be used to measure Γ_{2+} for I state RNA at Mg^{2+} concentrations which would otherwise induce folding to the N state. Second, we use a combination of experiment and computation to determine $\Delta\Delta G_{comp,2+}$ from the difference between ΔG_{I_E-2+} and G_{I_C-2+} (eq 5). There is no experimental method for trapping the distribution of conformers in the I_E or I_C ensemble as the Mg^{2+} concentration is varied. Instead, small-angle X-ray scattering (SAXS) measurements of R_g were used to detect compaction of A1088U RNA by Mg^{2+} in the same concentration range that induces folding of native sequences. Electrostatic calculations were then used to estimate $\Delta\Delta G_{comp,2+}$ from molecular models of the I state with dimensions corresponding to the experimental R_g at a C_{2+} equal to 0 or C^0_{2+}.

RESULTS

Measurements of Γ_{2+} for N and I State RNAs. We assess Mg^{2+}−RNA interactions by a fluorescence method that detects the effect of a RNA on the activity of Mg^{2+} ions (see Materials and Methods). The experimental quantity obtained is ΔC^{RNA}_{2+}, the "excess" Mg^{2+} (per RNA) needed to bring the Mg^{2+} activity in the presence of RNA to the same level as a reference solution without RNA. (ΔC^{nt}_{2+} is identical to ΔC^{RNA}_{2+}, only expressed as ions per nucleotide.) The Mg^{2+} concentration in the reference solution is the bulk Mg^{2+} concentration, C_{2+}. ΔC^{RNA}_{2+} approaches the thermodynamic quantity Γ_{2+} (defined in Materials and Methods, eq 3) under the experimental conditions used here.

ΔC^{nt}_{2+} has been measured for the two different variants of a 58-nucleotide *E. coli* rRNA domain shown in Figure 1. The mutation present in A1088U RNA prevents the formation of tertiary structure (*37*); UV melting experiments did not detect any new unfolding transitions when Mg^{2+} was added in the concentration ranges used in this work. At the lowest K^+ concentration that was used for ΔC^{nt}_{2+} measurements, 20 mM, the least stable secondary structure in this RNA unfolds with a T_m of ≈28 °C (Figure S2B of the Supporting Information). To avoid the possibility that titration with Mg^{2+} might induce some secondary structure folding, all measurements (and corresponding calculations) were performed at a temperature below the onset of this unfolding transition, 15 °C.

ΔC^{nt}_{2+} was measured for A1088U RNA at four different K^+ concentrations from 20 to 150 mM. Plots of ΔC^{nt}_{2+} versus $\log(C_{2+})$ show monotonic increases up to the maximum C_{2+} concentrations that were attained (Figure 3). Higher bulk Mg^{2+} levels are required to sustain a particular ΔC^{nt}_{2+} value as the K^+ concentration increases, as expected from competition between Mg^{2+} and K^+ ions for electrostatic interactions with the RNA. These curves are qualitatively similar to data obtained for homopolymer RNAs (*38*) or helical DNA (see below).

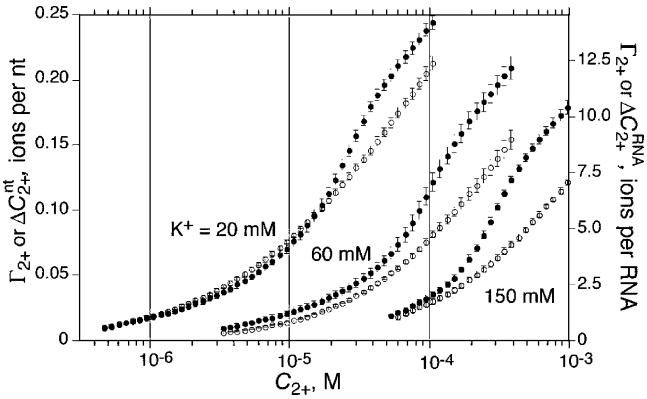

FIGURE 3: Excess Mg^{2+} measured for U1061A RNA (●) or A1088U RNA (○) at various concentrations of K^+. The ordinates are plotted in units of either ions per nucleotide (ΔC^{nt}_{2+}, left ordinate) or ions per RNA molecule (ΔC^{RNA}_{2+}, right ordinate). From left to right, titrations were carried out with a constant concentration of 20, 60, and 150 mM K^+, in standard buffer (see Materials and Methods). A fourth data set, collected at 40 mM K^+ and shown in Figures 6 and 7, has been omitted for clarity. Error bars are standard deviations from averages of five to seven data sets.

The second RNA variant examined is U1061A RNA, which has an exceptionally stable tertiary structure in the presence of Mg^{2+}, but no detectable tertiary structure when K^+ is the only cation present (*15*, *37*). Titration of this RNA with $MgCl_2$ is therefore expected to induce tertiary folding, and inflections in ΔC^{nt}_{2+} versus $\log(C_{2+})$ curves (Figure 3) suggest that a conformational transition to a form of the RNA with a larger ΔC^{nt}_{2+} takes place as C_{2+} is increased. Grilley et al. (*10*) showed that C_{2+} at the midpoint of the apparent transition in the 60 mM K^+ ΔC^{nt}_{2+} curve coincides with that of the folding transition followed by hyperchromicity at 295 nm, a wavelength that detects only the tertiary folding transition of this RNA (see Materials and Methods and Figure S1 of the Supporting Information). A similar coincidence of folding transitions monitored by UV absorbance and ΔC^{nt}_{2+} holds for the other K^+ concentrations as well (data not shown).

Under the experimental conditions of a large molar excess of KCl over $MgCl_2$, the area under a plot of ΔC^{nt}_{2+} versus $\log(C_{2+})$ is related to the free energy of Mg^{2+}−RNA interactions, ΔG_{RNA-2+} (eq 4). Extraction of such free energies from the ΔC^{nt}_{2+} curves in Figure 3 is complicated by the fact that the ensemble of A1088U RNA conformations is shifting to smaller average dimensions as the Mg^{2+} concentration increases (see R_g measurements in the next section), but as suggested by the diagrams in panels A and B of Figure 2, the ΔC^{nt}_{2+} observed for A1088U RNA will be between the ΔC^{nt}_{2+} values associated with the I_E and I_C ensembles (up to the Mg^{2+} concentration that defines I_C, C^0_{2+}). Thus, the apparent ΔG_{RNA-2+} obtained by integration of the ΔC^{nt}_{2+} curves is bracketed by the free energies we wish to estimate, ΔG_{I_E-2+} and ΔG_{I_C-2+} (Figure 2C and eq 5). These apparent free energies, evaluated at the transition midpoint, are compiled in Table 1. The probable range of free energies being averaged in this calculation is estimated below.

Table 1: Apparent Free Energies of Mg^{2+}-RNA Interactions with Partially Unfolded RNA[a]

		apparent ΔG_{RNA-2+} (kcal/mol)	
$[K^+]$ (mM)	C^0_{2+} (μM)	$C_{2+} = C^0_{2+}$	$C_{2+} = 1$ mM
20	28.0	−7.1	−
40	55.1	−4.8	−23.
60	95.8	−3.2	−14.
150	245	−2.0	−5.9

[a] Apparent free energies were calculated from ΔC^{nt}_{2+} vs $\log(C_{2+})$ data for A1088U RNA displayed in Figures 2 and 6A, using eq 4 of the text and integrating either to the midpoint of the tertiary folding transition in U1061A RNA ($C_{2+} = C^0_{2+}$) or to a C_{2+} of 1 mM. The transition midpoint was found from the inflection point of the ΔC^{nt}_{2+} vs $\log(C_{2+})$ data displayed in Figures 3 and 6. Because the ensemble of RNA conformations is changing during titration with $MgCl_2$, the free energies are averages of the more extended and compact ensembles present at low and high Mg^{2+} concentrations, respectively. See the text for further discussion.

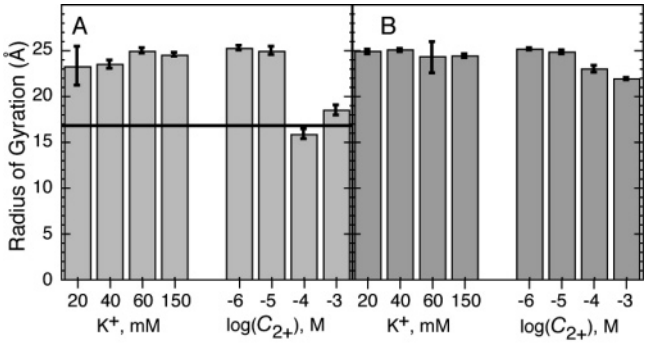

FIGURE 4: Radii of gyration measured in standard buffer at 15 °C for (A) U1061A RNA or (B) A1088U RNA. In each panel, the left four measurements were taken in the absence of Mg^{2+} and the right four measurements in the presence of 40 mM K^+. The horizontal bar is the R_g calculated from the coordinates of U1061A RNA in a crystal structure (PDB entry 1HQ8). Error bars are approximate uncertainties in the analysis of the data.

A1088U RNA as a Mimic of Partially Unfolded RNA. The ΔC^{nt}_{2+} curves for A1088U and U1061A RNAs approximately coincide at low Mg^{2+} concentrations that do not induce the U1061A RNA folding transition (Figure 3), providing evidence that A1088U RNA is an adequate mimic of the partially unfolded I state of U1061A RNA over the entire range of K^+ concentrations used in these experiments. Further support for the similar behavior of A1088U RNA and unfolded U1061A RNA was obtained from small-angle X-ray scattering (SAXS) measurements of R_g for the two RNAs under various conditions (Figure 4). Essentially the same R_g is measured for either RNA in the absence of Mg^{2+}, regardless of the K^+ concentration. A Mg^{2+} concentration which induces folding of U1061A RNA ($C_{2+} = 0.1$ mM in 40 mM K^+) causes the RNA to adopt a substantially more compact form in which the measured R_g (15.9 Å) is similar to that calculated from a crystal structure of the same RNA (16.9 Å) (*14*). [R_g appears to increase slightly at much higher Mg^{2+} concentrations, 1 mM; a similar increase has been seen with the *Tetrahymena* group I intron (*39*). This effect potentially reflects changes in the scattering properties of the ion atmosphere and solvent shell surrounding the RNA.] Even though the R_g for A1088U RNA does not change in the range of 20−150 mM K^+, a further small decrease (~2 Å) in R_g is seen at bulk Mg^{2+} concentrations that would induce folding of U1061A RNA, and a further 1 Å decrease at 1 mM C_{2+}. Thus, very low concentrations of Mg^{2+} (relative to the amount of K^+ present) enable the partially unfolded RNA to adopt conformations more compact than those observed with K^+ alone.

Models of Partially Unfolded RNA. As suggested above, the apparent ΔG_{RNA-2+} calculated from data obtained with A1088U RNA lies between ΔG_{I_E-2+} and ΔG_{I_C-2+}. Because there is no experimental method for estimating how large the difference between these two free energies might be, we used a computational approach to answer this question. First, we generated a set of 129 molecular models containing only secondary structure and random conformations at the helix junction (see Materials and Methods). R_g values from ~19 to 25 Å are represented within the set. Experimental R_g values were in a similar range, from ~22 to 25 Å, suggesting that the models have sampled an appropriate range of conformations. The models were then sorted by decreasing R_g to correspond to the average configurational states of the different I state ensembles present at increasing C_{2+} values, using the SAXS measurements for A1088U RNA (Figure 4B) to relate R_g values to specific Mg^{2+} concentrations. Finally, the free energy of interaction of Mg^{2+} with each model was calculated from solutions to the NLPB equation (see Materials and Methods). In this section, we present the structural models and NLPB-based calculations; Mg^{2+}−RNA interaction free energies are estimated in a following section.

For the different sets of models sorted by 1 Å increments in R_g, we find that the average calculated value of Γ_{2+} decreases as R_g increases. This trend is seen in panels A and B of Figure 5; for instance, the Γ_{2+} curve averaged from RNAs with smaller R_g values (20−21 Å) lies above the curve for RNAs with larger R_g values (24−25 Å). The RNA models with large R_g values exhibit a relatively narrow range of Γ_{2+} (Figure 5A). Presumably, the RNA models with the largest R_g have extended single strands that position the helices as far apart as possible; such models approach the lowest possible charge density and correspondingly small values of Γ_{2+}. In contrast, RNAs having a more compact overall conformation have access to a greater variety of junction configurations and a larger variation in the electrostatic potentials surrounding the RNA, which may account for the wider Γ_{2+} range among RNAs with smaller R_g values (Figure 5B).

Another way to view the correlation between Γ_{2+} and R_g among the models is shown in Figure 5C, which plots Γ_{2+} as a function of R_g at different C_{2+} values chosen to bracket the Mg^{2+} concentration range over which the U1061A RNA folding transition takes place. I state models with a smaller R_g have larger Γ_{2+} values, on average. These trends suggest that increasing Mg^{2+} concentrations will favor an ensemble of I state conformations with a smaller average R_g. This conclusion qualitatively agrees with R_g measurements on A1088U RNA (Figure 4), which showed R_g decreasing from 25 Å in the absence of Mg^{2+} to 22 Å when C_{2+} reaches 1 mM.

Comparison of NLPB-Based Calculations with Experiment. Before estimating Mg^{2+}−RNA interaction free energies for different I state ensembles, we first show in this section that NLPB-based calculations of Γ_{2+} consistently underestimate experimentally measured ΔC^{nt}_{2+} values but that the

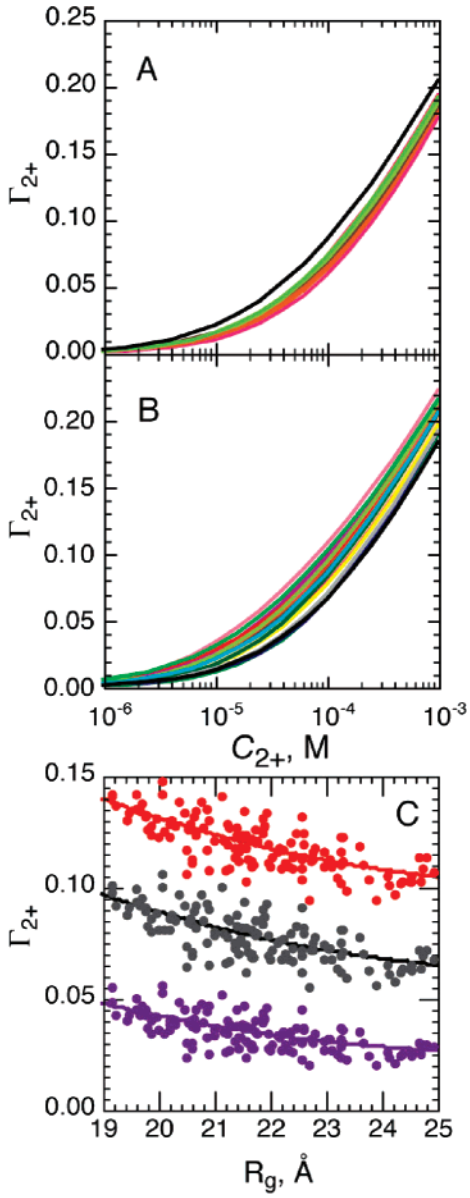

FIGURE 5: NLPB-based calculations of Γ_{2+} for models of A1088U RNA, at a monovalent cation concentration of 40 mM and 15 °C. (A) Colored curves are calculated for the 13 structures with R_g values ranging from 24 to 25 Å. The black line is the average of curves calculated from models with R_g values ranging between 20 and 21 Å (B). (B) Colored curves are calculated for the 19 structures with R_g values ranging between 20 and 21 Å. The black line is the average of curves calculated from models with R_g values ranging between 24 and 25 Å (A). (C) Calculated values of Γ_{2+} for all 129 models at C_{2+} values of 251 (red), 100 (gray), and 25.1 μM (purple). The curves are least-squares fits of second-order polynomials to the data; they have no physical significance and are intended only as a qualitative indication of the correlation between Γ_{2+} and R_g.

difference ($\Delta\Gamma_{2+} = \Gamma^{N}_{2+} - \Gamma^{I}_{2+}$) can be reliably calculated (next section). We start with calculated Γ_{2+} curves for the folded state of the RNA (Figure 6) (see Materials and Methods). We have previously suggested that chelation of a Mg^{2+} ion between a nonbridging phosphate oxygen of A1073 and O4 of U1094 contributes a substantial free energy to the folding reaction (*6*). To show the effect the occupancy of this chelation site would have on Γ_{2+}, NLPB calculations have been conducted with or without an ion fixed at this site (solid and dashed lines, respectively, in Figure 6). As

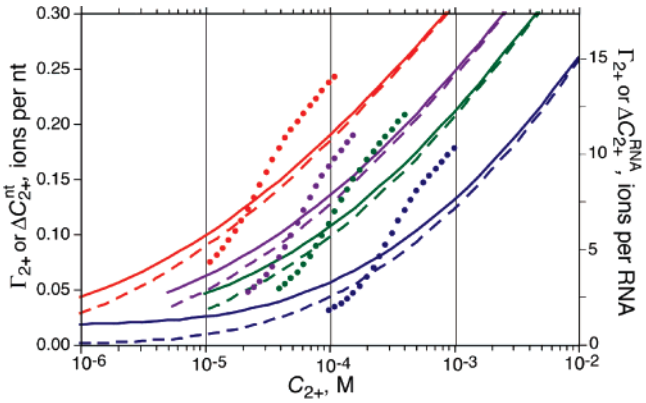

FIGURE 6: NLPB-based calculations of Γ_{2+} for folded U1061A RNA. Dashed lines were calculated using crystal structure coordinates of the RNA only (PDB entry 1HC8); the solid line was calculated with a Mg^{2+} ion fixed at a single site in the RNA (*6*). Dots are experimental data for U1061A RNA taken from Figure 3; data at C_{2+} below the folding transition are not shown for clarity. Sets of data and calculated curves were obtained in buffers containing different concentrations of K^+: (red) 20, (purple) 40, (green) 60, and (blue) 150 mM.

C_{2+} becomes smaller, Γ_{2+} approaches one ion per RNA for the curves calculated with a chelated Mg^{2+}, while at high C_{2+} values, the effect of the chelated ion on Γ_{2+} becomes negligible. (This observation is related to the strong interactions taking place between Mg^{2+} ions in different RNA environments; see the Discussion for further comments.)

ΔC^{nt}_{2+} data for U1061A RNA are also displayed in Figure 6. At the highest Mg^{2+} ion concentrations, the data represent interactions of the ion with only the folded (N) state of the RNA and parallel the corresponding curve calculated by NLPB methods, though the calculated curves consistently underestimate the measurements. Note that Γ_{2+} is relatively insensitive to assumptions about the occupancy of the chelated site at Mg^{2+} concentrations large enough to induce folding to the N state.

Further comparisons of calculated Γ_{2+} curves with measurements are presented in Figure 7. NLPB-based calculations using A1088U RNA models underestimate the measured ΔC^{nt}_{2+} curves for the RNA (Figure 7A), and the discrepancy between Γ_{2+} and ΔC^{nt}_{2+} increases with C_{2+}. (The comparison shown is at 40 mM K^+, but similar differences between data and calculations are seen at other salt concentrations.) A possible explanation for this increasing divergence is that A1088U RNA becomes more compact (and thus is associated with progressively larger ΔC^{nt}_{2+}) as C_{2+} increases, while the calculations are based on static models. Under the same buffer conditions (40 mM K^+), there is a much closer parallel between calculated and experimental excess Mg^{2+} curves for helical DNA (Figure 7B). It is noteworthy that ΔC^{nt}_{2+} curves for DNA and A1088U RNA are quite different in shape: the RNA is associated with a larger number of excess Mg^{2+} ions, especially at low C_{2+} values. The larger value of Γ_{2+} implies that the charge density of the RNA helix junction is higher than that of helical DNA.

Comparison of Calculated and Measured $\Delta\Gamma_{2+}$ *Values.* We now combine the data and calculations presented in Figures 6 and 7 to obtain $\Delta\Gamma_{2+}$, the difference between Γ^{N}_{2+} and Γ^{I}_{2+}. This difference determines the sensitivity of a RNA folding reaction to changes in Mg^{2+} concentration and

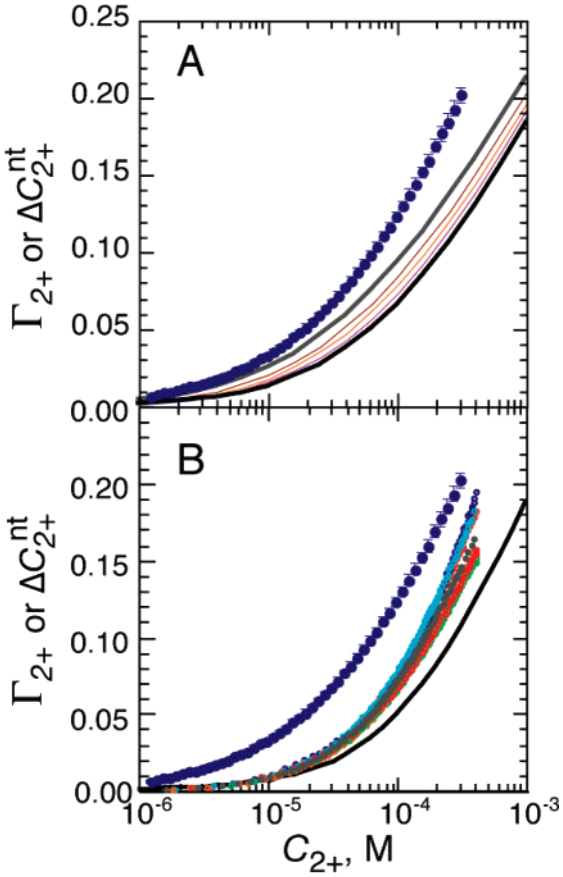

FIGURE 7: Comparison of experimental and calculated excess Mg^{2+} curves at 40 mM K^+. (A) ΔC^{nt}_{2+} for A1088U RNA (blue dots). The solid lines are NLPB-based calculations of Γ_{2+} from A1088U RNA models with different ranges of R_g; from the gray to black lines, the ranges are 19−20, 20−21, 21−22, 22−23, and 24−25 Å. (B) Seven independent determinations of $\Delta C^{nt}_{Mg^{2+}}$ for helical DNA at 40 mM K^+ (colored data points). For comparison, the A1088U RNA data from panel B are shown (dark blue points). The black curve is Γ_{2+} calculated for helical DNA using a cylindrical model (see Materials and Methods).

can also be derived from linkage analysis (eq 1) without directly measuring Γ_{2+}. Because $\Delta\Gamma_{2+}$ is a relatively small difference between large numbers, it is sensitive to small changes in Γ^I_{2+} and a good test of the adequacy of our I state models.

Figure 8 compares calculated values of $\Delta\Gamma_{2+}$ with two different experimental determinations of the same quantity. A family of $\Delta\Gamma_{2+}$ curves is plotted, in which the I state models used in the NLPB calculations were taken from those with R_g values in the range of 19−20 Å (smallest $\Delta\Gamma_{2+}$) up to 24−25 Å (largest $\Delta\Gamma_{2+}$). (Because there is good evidence for a chelated ion in the folded RNA, only the curves calculated with a single Mg^{2+} fixed in the N state structure are shown. Without the fixed ion, $\Delta\Gamma_{2+}$ is smaller by ~0.017 ion/nucleotide at a C_{2+} of 10^{-6} M or by 0.0037 at a C_{2+} of 10^{-3} M.) Depending on the set of I state models used in the calculations, the maximum value of $\Delta\Gamma_{2+}$ varies by nearly 2-fold. To indicate the degree to which compaction of the I state by Mg^{2+} affects the shape of the $\Delta\Gamma_{2+}$ curve, a red dot is placed on the Γ_{2+} curve calculated from I state models with an R_g in the same range as that measured at the corresponding C_{2+}. At a C_{2+} of 1 mM, compaction of the RNA is estimated to decrease $\Delta\Gamma_{2+}$ by ~20% over what

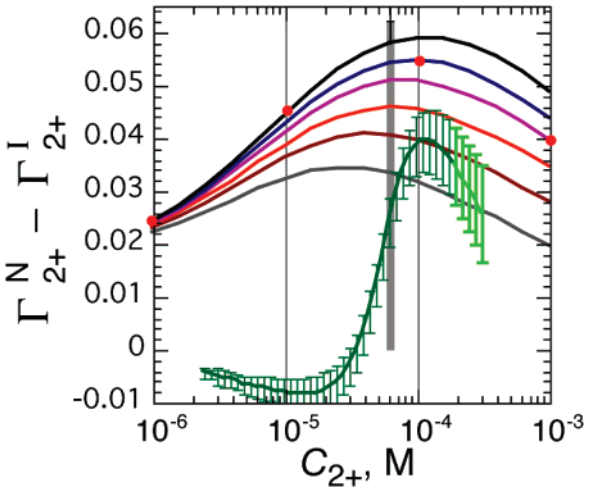

FIGURE 8: Differences in the amount of excess Mg^{2+} between native and I state RNA, as deduced from calculations or experiment. All calculations and experiments refer to buffer with 40 mM K^+. The solid curves are the differences between NLPB-based calculations of Γ_{2+} for folded U1061A RNA (Figure 6, including a chelated ion) and Γ_{2+} calculated for A1088U models in various ranges of R_g; from the gray to black curves, the ranges used are 19−20 (gray), 20−21 (brown), 21−22, 22−23 (orange), 23−24 (blue), and 24−25 Å (black). The green points with error bars are the differences between ΔC^{nt}_{2+} values measured with U1061A and A1088U RNAs. Light green points are within the C_{2+} range for which U1061A is fully folded, and the data correspond to $\Delta\Gamma_{2+}$. The vertical gray line (with an error bar) at a C_{2+} of 55 μM is $\Delta\Gamma_{2+}$ derived by linkage analysis from UV-monitored folding of U1061A RNA (see the text). Red dots are placed on the calculated curves whose R_g range corresponds to the measured R_g measured at the indicated C_{2+} (Figure 4).

would be observed if the I state ensemble maintained the same dimensions as Mg^{2+} is added.

The experimental quantity corresponding to $\Delta\Gamma_{2+}$, $\Delta(\Delta C^{nt}_{2+})$ calculated from the difference between ΔC^{nt}_{2+} for U1061A and A1088U RNAs, is plotted with error bars in Figure 8. Because U1061A RNA is completely folded only at higher Mg^{2+} concentrations, $\Delta(\Delta C^{nt}_{2+})$ can be compared with $\Delta\Gamma_{2+}$ only when $C_{2+} > \sim 0.2$ mM (light green data points). The data fall below the calculated curves, though the associated errors are fairly large. $\Delta\Gamma_{2+}$ has also been determined from linkage analysis of the extent of RNA folding (monitored by UV absorption) as a function of $\ln(C_{2+})$ (eq 1) (data not shown; a similar measurement of $\Delta\Gamma_{2+}$ at 60 mM K^+ is in ref *10*). This approach gives a $\Delta\Gamma_{2+}$ of 0.062 ± 0.009 ion/nucleotide from data collected in buffers containing 40 mM K^+. This $\Delta\Gamma_{2+}$ value is shown as a vertical bar at the transition midpoint in Figure 8; it is within experimental error of the calculated value. The reasonable agreement between calculated and experimental values of $\Delta\Gamma_{2+}$ suggests that NLPB-based calculations, despite their tendency to underestimate Γ_{2+}, are adequate for finding differences between interactions of Mg^{2+} with different RNA states and that our I state molecular models are acceptable representations of the electrostatic properties of the I state (see the Discussion for further comment).

Estimation of the Free Energy of Interaction of Mg^{2+} with Partially Folded RNA Structures. We now use the I state models to estimate the difference in Mg^{2+} interaction free energies between extended and compact I state ensembles, $\Delta G_{comp,2+}$ (Figure 2 and eq 4). These calculations were all

carried out at a K^+ concentration of 40 mM. On the basis of the SAXS measurements, we used models with R_g values in the range of 24−25 Å to represent the extended ensemble in the absence of Mg^{2+}, I_E, and models with R_g values smaller by 2 Å (22−23 Å) to represent I_C at the C_{2+} needed to fold tertiary structure (55 μM Mg^{2+}). The difference between the corresponding calculated free energies of Mg^{2+} interaction, $\Delta G_{I_C-2+} - \Delta G_{I_E-2+}$, gave a $\Delta\Delta G_{comp,2+}$ of −0.5 kcal/mol of RNA. In a second calculation, we estimated $\Delta\Delta G_{comp,2+}$ for compaction at a C_{2+} of 1 mM Mg^{2+}, at which point R_g has been reduced by 3 Å (to the 21−22 Å range). $\Delta\Delta G_{comp,2+}$ became more favorable, −2.0 kcal/mol of RNA. The wild-type *E. coli* sequence of this 58-nucleotide rRNA fragment requires a C_{2+} approximately 1 order of magnitude higher to fold tertiary structure compared to that of U1061A RNA [∼2 mM Mg^{2+} in the presence of 100 mM KCl (*40*)]. Thus, the more negative value of $\Delta G_{comp,2+}$ at 1 mM Mg^{2+} is potentially relevant to the folding of natural rRNA sequences.

An important question for these electrostatic calculations is whether the sets of models, selected solely on the basis of their R_g values, are representative of the most common RNA conformations present in solution at different Mg^{2+} concentrations. If Mg^{2+} interacts more strongly with conformations having a higher charge density, then among models with similar R_g values, those having larger Γ_{2+} values are perhaps better representations of the compacted state. To see how serious this problem might be, we repeated calculations of $\Delta\Delta G_{comp,2+}$ using only the two models with the largest Γ_{2+} in either the 21−22 or 22−23 Å set of models. The estimate of $\Delta\Delta G_{comp,2+}$ at the U1061A RNA transition midpoint, 55 μM Mg^{2+}, nearly doubles to −0.9 kcal/mol of RNA. $\Delta\Delta G_{comp,2+}$ at 1 mM Mg^{2+} is also more negative, −3.0 kcal/mol of RNA.

The apparent experimental value of ΔG_{RNA-2+} for A1088U RNA, −4.8 kcal/mol at 40 mM K^+ and 55 μM Mg^{2+} (Table 1), is 5−10 times more negative than the difference $\Delta\Delta G_{comp,2+}$ (between −0.5 and −0.9 kcal/mol). Since ΔG_{RNA-2+} must be bracketed by ΔG_{I_E-2+} and ΔG_{I_C-2+} (Figure 2A), we estimate that the latter two free energies fall in the ranges of −4.4 to −4.6 kcal/mol and −5.0 to −5.2 kcal/mol, respectively. These free energies are compared with other Mg^{2+}-dependent free energies of folding in the Discussion.

DISCUSSION

Measurement of Γ_{2+} and ΔG_{RNA-2+} for I State RNA Ensembles. This study attempts to quantitate the Mg^{2+}−RNA interaction energies relevant to the folding of tertiary structure in a 58mer rRNA fragment. Three states of the RNA are of particular interest: the I state ensemble of conformations stabilized by monovalent cations in the absence of Mg^{2+} (I_E), the I state ensemble of more compact conformations from which tertiary structure is formed at Mg^{2+} concentrations near the folding transition midpoint (I_C), and the folded state itself (N). To take experimental measurements on the I state RNA, we used a RNA variant unable to fold to the tertiary structure (A1088U RNA). In the presence of Mg^{2+} concentrations too low to induce tertiary folding of U1061A RNA, Γ_{2+} values for the two RNAs are the same (within experimental error) at all monovalent salt concentrations, and the radii of gyration for the two RNAs (measured at 40 mM K^+) are also within error. We therefore suppose that formation of U1061A RNA tertiary structure takes place from an ensemble of conformations with properties similar to those of A1088U RNA.

Our measurements with A1088U RNA (Figures 3 and 7) represent one of the few sets of data available on the interactions of Mg^{2+} with partially unfolded RNA configurations [other studies have examined homopolymer RNAs (*11*, *38*, *41*, *42*) and the partially unfolded states of a pseudoknot (*11*) and tRNA (*43*)]. Two comments about these data are in order. First, the apparent Mg^{2+}−RNA interaction free energies (Table 1) are strongly dependent on the concentration of competing monovalent ion, as expected, but remain favorable by several kilocalories per mole of RNA even at 150 mM K^+. This result is consistent with recent experiments on a partially unfolded group I intron RNA, which showed significant interactions with Mg^{2+} persisting at a very high salt concentration, 2 M NaCl (*43*). Interactions of Mg^{2+} with the I state are thus important over a wide range of solution conditions.

A second important feature of the interactions of Mg^{2+} with A1088U RNA is that Γ_{2+} for this I state RNA mimic is larger than for helical DNA under the same buffer conditions (Figure 7B). At the RNA folding transition midpoint (55 μM Mg^{2+} in 40 mM K^+), the Γ_{2+} of 0.088 for A1088U RNA is approximately halfway between the Γ_{2+} of 0.048 for DNA and the Γ_{2+} of ≈0.013 estimated for the folded RNA. Thus, the helix junction in the I state must have a much higher charge density than a simple helix, a conclusion which may be related to the R_g of the I state being more sensitive to Mg^{2+} than K^+ (see below). It is plausible that the I state ensembles for different RNAs could display distinctly different Γ_{2+} profiles, depending for instance on the way helical segments are joined in junctions. Realistic models of the I state for a specific RNA sequence are therefore important in assessing the effects of Mg^{2+} on RNA folding.

Influence of K^+ and Mg^{2+} on the I State Ensemble. SAXS measurements of A1088U RNA (Figure 4) indicate that low concentrations of Mg^{2+} (in the presence of a large excess of K^+) cause a small degree of compaction of the I state ensemble. No effect of K^+ on R_g on the RNA was detected over a wide range of concentrations, 20−150 mM. It is unlikely that the distribution of conformations in the I state ensemble is completely insensitive to K^+ concentration; we conclude from these results only that Mg^{2+} is simply much more effective than K^+ at reducing R_g. We have previously argued that the sensitivity of tRNA stability to Mg^{2+} is related to the fact that the entropic cost of bringing a divalent ion into the ion atmosphere of a RNA is more than offset by the entropic advantage of "releasing" approximately two monovalent ions to the bulk solution (*36*). This entropic advantage becomes larger as the charge density of the RNA increases and the ion atmosphere is held closer (on average) to the RNA. Because a relatively high charge density (reflected in high values of Γ_{2+}) was observed for the I state mimic RNA, it is plausible that Mg^{2+} is more effective than K^+ in promoting compaction of the RNA.

SAXS and analytical ultracentrifugation studies of some other RNAs have observed 20−30% decreases in R_g with increasing monovalent cation concentrations (*44*−*46*), and in some cases, $MgCl_2$ addition may decrease the R_g of partially unfolded RNAs by 20−40% without causing a

complete set of tertiary interactions to form (*44*−*48*). There are several possible reasons why much smaller effects are seen in the experiments reported here. One is that the our measurements with the rRNA fragment were taken under conditions in which there was no net gain in secondary structure as K^+ or Mg^{2+} concentrations were increased. (Titration of the U1061A RNA with $MgCl_2$ under salt and temperature conditions only a little less stabilizing than those reported in Figure 4 does result in substantial secondary structure formation before the onset of tertiary structure folding; cf. Figure S3 of the Supporting Information.) Although structure mapping experiments have suggested that most of the secondary structure of the *Tetrahymena* group I intron is intact at low monovalent salt concentrations (*49*), in some of the cited studies stabilization of secondary structure by the added ions may be influencing R_g. All the RNAs showing a large degree of compaction of the I state in response to ions are also substantially larger than the 58mer studied here. Either the overall size or the topological complexity (e.g., the number and size of helix junctions) might influence the magnitude of the changes in R_g. Larger RNAs may also have more complex responses to Mg^{2+}, in that intermediates with partial sets of tertiary interactions are more likely (*48*, *50*).

Calculation of the Difference in ΔG_{RNA-2+} for Extended and Compact I State Ensembles. To ask how much more strongly Mg^{2+} interacts with A1088U RNA as its dimensions decrease, we had to rely on electrostatic calculations with I state molecular models. Two sets of concerns arise in relation to these calculations. One is the reliability of the NLPB equation for obtaining Mg^{2+}−RNA interaction free energies. There is good agreement between NLPB-based calculations and experimental data for duplex RNA, tRNA, and a pseudoknot RNA (*11*, *36*, *51*). In all these cases, the free energies of Mg^{2+} interactions are dominated by diffuse (hydrated) ions. NLPB-based calculations tend to underestimate the excess Mg^{2+} ions neutralizing nucleic acid charge (Γ_{2+}) in comparisons with experiments (Figure 7 and ref *11*) and in comparison with theoretical calculations that take into account ion size (*52*). Nevertheless, free energy differences, including the salt dependence of peptide−RNA interactions (*53*), p*K* shifts in a DNA-binding drug (*54*), and the Mg^{2+}-dependent difference in free energy between two RNA conformations (*11*) have been reliably calculated from the NLPB equation. We do not expect expanded and compact forms of the I state ensemble to interact with Mg^{2+} by very different mechanisms and therefore expect the free energy difference calculated for interactions of Mg^{2+} with sets of models representing the I_E and I_C states, $\Delta\Delta G_{comp,2+}$, to be reliable.

A second concern is whether the sets of molecular models used in the NLPB calculations represent the most probable members of the statistical ensembles of RNA conformations present at a particular Mg^{2+} concentration. R_g was the only criterion for selecting the models corresponding to a set of solution conditions, and as a global measure of RNA dimensions, it provides only a rough discrimination as to which models should be considered representative. Experimental methods that measure the distributions of distances present in a RNA, such as single-molecule fluorescence energy transfer (*55*), might provide additional criteria for selecting the most representative models. In the absence of such information, we argue that the models with the largest Γ_{2+} values at a given R_g will set a limit for the lowest possible Mg^{2+}−I state interaction free energy.

For the 58mer rRNA fragment studied here, our computations suggest that the tendency of the partially unfolded ensemble to adopt more compact conformations enhances their free energies of interaction with Mg^{2+} by a maximum of ∼20%. This is a relatively small increment, but the resulting free energy could be a significant factor in determining the stabilization of a RNA by Mg^{2+} (see below).

Implications of Interactions of Mg^{2+} with the RNA I State for Folding to the N State. We previously estimated that Mg^{2+} stabilizes the U1061A RNA N state by approximately −23 kcal/mol relative to the ensemble of I states present at the midpoint of the folding transition (15 °C, 0.1 mM Mg^{2+}, 60 mM K^+) (*10*). This free energy, $\Delta\Delta G_{fold,2+}$, is only ∼0.4 kcal/mol more negative under the conditions considered here (55 μM Mg^{2+}, 40 mM K^+). The comparable difference in Mg^{2+} interaction free energies between the I_C and I_E states, $\Delta\Delta G_{comp,2+}$, is at most 5% of this value.

In the introductory section, two extreme cases for the way the addition of Mg^{2+} to a RNA solution might promote folding were posed. Mg^{2+} could interact much more strongly with compact conformations of the I state so that tertiary structure is formed from RNA conformations with dimensions and charge densities not much different than those of the native conformation (Figure 2B), or Mg^{2+} could have relatively little influence on the I state conformations but strongly stabilize the N state (Figure 2A). The 58mer RNA studied here seems to fall into the latter category. R_g decreases significantly in response to Mg^{2+}, by as much as 15%, but folding to the N state is accompanied by a further ∼28% decrease in R_g. Likewise, the estimated free energy difference in Mg^{2+} interactions between compact and extended conformations is significant, as much as −1 kcal/mol, but small compared to the nearly −20 kcal/mol difference in Mg^{2+} interaction free energies between the N and I state RNAs.

Although the degree of compaction of the rRNA fragment caused by addition of Mg^{2+} is small, it nevertheless represents a significant change in RNA dimensions and charge density. As pointed out above, the 58mer RNA fragment is small and has only a single helix junction influencing the dimensions and flexibility of the molecule. It will be interesting to see how the free energies of interactions of Mg^{2+} with larger RNA folding intermediates compare to those observed for the rRNA fragment reported here.

Discrimination between Models of Ion−RNA Interaction using Γ_{2+}. Calculations based on the NLPB equation are in good agreement with the experimentally determined values of $\Delta\Gamma_{2+}$ for 58mer RNA folding (Figure 8). As $\Delta\Gamma_{2+}$ (or a similar quantity, the Hill coefficient) has in the past been interpreted as a measure of the number of Mg^{2+} ions binding to specific sites in the native RNA structure (*56*), the significance of this agreement requires comment. The calculations used an N state model that includes a chelated ion in the structural coordinates. As seen in the Γ_{2+} curves in Figure 6, as a larger fraction of the N state RNA charge is neutralized by Mg^{2+}, the Γ_{2+} values become less sensitive to the presence or absence of a chelated ion within the structure, and when C_{2+} is large, the calculated values of

Γ_{2+} are nearly the same whether a chelated ion has been included. The reason for this behavior of the Γ_{2+} curves is the strong repulsive interaction between a site-bound ion and diffuse ions, which reduces the number of the latter (*9*). The net result is that calculations with or without a site-bound ion present differ in Γ_{2+} by only 0.007 ion/nucleotide at C_{2+} near the folding transition midpoint (Figure 8). This difference is within the error of the experimental measurements.

In contrast, $\Delta\Gamma_{2+}$ is very sensitive to the model used for the I state. For instance, if helical DNA had been used instead of the structural models, $\Delta\Gamma_{2+}$ would have been estimated as ~0.10 ion/nucleotide at C_{2+} of the transition midpoint (Figure 8), approximately twice the actual value. There is also a nearly 2-fold variation in Γ_{2+} when I state models with different radii of gyration are used. The agreement between calculations and experiments in Figure 8 is therefore good evidence that our I state models are reasonable but does not support a specific model of interactions of Mg^{2+} with the folded state.

SUPPORTING INFORMATION AVAILABLE

Melting profile for U1061A RNA (Figure S1), melting profiles of U1061A and A1088A RNA (Figure S2), and normalized absorbance changes for U1061A RNA titrated with $MgCl_2$ (Figure S3). This material is available free of charge via the Internet at http://pubs.acs.org.

REFERENCES

1. Cole, P. E., Yang, S. K., and Crothers, D. M. (1972) Conformational Changes of Transfer Ribonucleic Acid. Equilibrium Phase Diagrams, *Biochemistry 11*, 4358−4368.
2. Fang, X., Pan, T., and Sosnick, T. R. (1999) A thermodynamic framework and cooperativity in the tertiary folding of a Mg^{2+}-dependent ribozyme, *Biochemistry 38*, 16840−16846.
3. Stein, A., and Crothers, D. M. (1976) Conformational Changes of Transfer RNA. The Role of Magnesium(II), *Biochemistry 15*, 160−167.
4. Draper, D. E., Grilley, D., and Soto, A. M. (2005) Ions and RNA folding, *Annu. Rev. Biophys. Biomol. Struct. 34*, 221−243.
5. Grilley, D., Soto, A. M., and Draper, D. E. (2007) Direct quantitation of Mg^{2+}−RNA interactions by use of a fluorescent dye, *Methods Enzymol.*, in press.
6. Misra, V. K., and Draper, D. E. (2001) A thermodynamic framework for Mg^{2+} binding to RNA, *Proc. Natl. Acad. Sci. U.S.A. 98*, 12456−12461.
7. van Buuren, B. N., Hermann, T., Wijmenga, S. S., and Westhof, E. (2002) Brownian-dynamics simulations of metal-ion binding to four-way junctions, *Nucleic Acids Res. 30*, 507−514.
8. Petrov, A. S., Lamm, G., and Pack, G. R. (2005) Calculation of the binding free energy for magnesium-RNA interactions, *Biopolymers 77*, 137−154.
9. Misra, V. K., and Draper, D. E. (2002) The linkage between magnesium binding and RNA folding, *J. Mol. Biol. 317*, 507−521.
10. Grilley, D., Soto, A. M., and Draper, D. E. (2006) Mg^{2+}-RNA interaction free energies and their relationship to the folding of RNA tertiary structures, *Proc. Natl. Acad. Sci. U.S.A. 103*, 14003−14008.
11. Soto, A. M., Misra, V., and Draper, D. E. (2007) Tertiary structure of an RNA pseudoknot is stabilized by "diffuse" Mg^{2+} ions, *Biochemistry 46*, 2973−2983.
12. Schneider, N. S., and Doty, P. (1954) Macro-Ions IV. The ionic strength dependence of the molecular properties of sodium carboxymethylcellulose, *J. Phys. Chem. 58*, 762−769.
13. Buchmueller, K. L., Webb, A. E., Richardson, D. A., and Weeks, K. M. (2000) A collapsed non-native RNA folding state, *Nat. Struct. Biol. 7*, 362−366.
14. Conn, G. L., Draper, D. E., Lattman, E. E., and Gittis, A. G. (1999) Crystal structure of a conserved ribosomal protein-RNA complex, *Science 284*, 1171−1174.
15. Lu, M., and Draper, D. E. (1994) Bases Defining an Ammonium and Magnesium Ion-Dependent Tertiary Structure Within the Large Subunit Ribosomal RNA, *J. Mol. Biol. 244*, 572−585.
16. Gurevich, V. V. (1996) Use of bacteriophage RNA polymerase in RNA synthesis, *Methods Enzymol. 275*, 382−397.
17. He, B., Rong, M., Lyakhov, D., Gartenstein, H., Diaz, G., Castagna, R., McAllister, W. T., and Durbin, R. K. (1997) Rapid mutagenesis and purification of phage RNA polymerases, *Protein Expression Purif. 9*, 142−151.
18. Conn, G. L., Gittis, A. G., Lattman, E. E., Misra, V. K., and Draper, D. E. (2002) A compact RNA tertiary structure contains a buried backbone-K^+ complex, *J. Mol. Biol. 318*, 963−973.
19. Xing, Y., and Draper, D. E. (1995) Stabilization of a ribosomal RNA tertiary structure by ribosomal protein L11, *J. Mol. Biol. 249*, 319−331.
20. Blyn, L. B., Risen, L. M., Griffey, R. H., and Draper, D. E. (2000) The RNA-binding domain of ribosomal protein L11 recognizes an rRNA tertiary structure stabilized by both thiostrepton and magnesium ion, *Nucleic Acids Res. 28*, 1778−1784.
21. Shiman, R., and Draper, D. E. (2000) Stabilization of RNA tertiary structure by monovalent cations, *J. Mol. Biol. 302*, 79−91.
22. Svergun, D. I., Semenyuk, A. V., and Feigin, L. A. (1988) Small-Angle-Scattering Data Treatment by the Regularization Method, *Acta Crystallogr. A44*, 244−250.
23. Schwieters, C. D., Kuszewski, J. J., Tjandra, N., and Clore, G. M. (2003) The Xplor-NIH NMR molecular structure determination package, *J. Magn. Reson. 160*, 65−73.
24. Wang, Y. X., Huang, S., and Draper, D. E. (1996) Structure of a U·U pair within a conserved ribosomal RNA hairpin, *Nucleic Acids Res. 24*, 2666−2672.
25. Wang, Y.-X., Huang, S., and Draper, D. E. (1995) Structure of a a U·U within a conserved ribosomal RNA hairpin, *Nucleic Acids Res. 24*, 2666−2672.
26. Huang, S., Wang, Y. X., and Draper, D. E. (1996) Structure of a Hexanucleotide RNA Hairpin Loop Conserved in Ribosomal RNAs, *J. Mol. Biol. 258*, 308−321.
27. Laing, L. G., and Draper, D. E. (1994) Thermodynamics of RNA Folding in a Highly Conserved Ribosomal RNA Domain, *J. Mol. Biol. 237*, 560−576.
28. Zuker, M. (2003) Mfold web server for nucleic acid folding and hybridization prediction, *Nucleic Acids Res. 31*, 3406−3415.
29. Svergun, D. I., Barberato, C., and Koch, M. J. H. (1995) CRYSOL: A program to evaluate X-ray solution scattering of biological macromolecules from atomic coordinates, *J. Appl. Crystallogr. 25*, 495−503.
30. Lu, X. J., and Olson, W. K. (2003) 3DNA: A software package for the analysis, rebuilding and visualization of three-dimensional nucleic acid structures, *Nucleic Acids Res. 31*, 5108−5121.
31. Chen, S. W., and Honig, B. (1997) Monovalent and Divalent Salt Effects on Electrostatic Free Energies Defined by the Nonlinear Poisson-Boltzmann Equation: Application to DNA Binding Reactions, *J. Phys. Chem. B 101*, 9113−9118.
32. Sharp, K. A., Friedmman, R. A., Misra, V., Hecht, J., and Honig, B. (1995) Salt effects on polyelectrolyte-ligand binding: Comparison of Poisson-Boltzmann, and limiting law/counterion binding models, *Biopolymers 36*, 245−262.
33. Gilson, M. K., and Honig, B. H. (1986) The dielectric constant of a folded protein, *Biopolymers 25*, 2097−2119.
34. Misra, V. K., Hecht, J. L., Yang, A. S., and Honig, B. (1998) Electrostatic contributions to the binding free energy of the lambda cI repressor to DNA, *Biophys. J. 75*, 2262−2273.
35. Misra, V. K., Sharp, K. A., Friedman, R. A., and Honig, B. (1994) Salt Effects on Ligand-DNA Binding: Minor Groove Binding Antibiotics, *J. Mol. Biol. 238*, 245−263.
36. Misra, V. K., and Draper, D. E. (2000) Mg^{2+} binding to tRNA revisited: The nonlinear Poisson-Boltzmann model, *J. Mol. Biol. 299*, 813−825.
37. Maeder, C., Conn, G. L., and Draper, D. E. (2006) Optimization of a ribosomal structural domain by natural selection, *Biochemistry 45*, 6635−6643.
38. Krakauer, H. (1974) A Thermodynamic Analysis of the Influence of Simple Mono- and Divalent Cations on the Conformational Transitions of Polynucleotide Complexes, *Biochemistry 13*, 2579−2589.
39. Russell, R., Millett, I. S., Doniach, S., and Herschlag, D. (2000) Small angle X-ray scattering reveals a compact intermediate in RNA folding, *Nat. Struct. Biol. 7*, 367−370.

40. Laing, L. G., Gluick, T. C., and Draper, D. E. (1994) Stabilization of RNA Structure by Mg^{2+} Ion: Specific and Non-specific Effects, *J. Mol. Biol. 237*, 577−587.
41. Krakauer, H. (1971) The Binding of Mg^{2+} Ions to Polyadenylate, Polyuridylate, and Their Complexes, *Biopolymers 10*, 2459−2490.
42. Römer, R., and Hach, R. (1975) tRNA conformation and magnesium binding. A study of a yeast phenylalanine-specific tRNA by a fluorescent indicator and differential melting curves, *Eur. J. Biochem. 55*, 271−284.
43. Das, R., Travers, K. J., Bai, Y., and Herschlag, D. (2005) Determining the Mg^{2}+ stoichiometry for folding an RNA metal ion core, *J. Am. Chem. Soc. 127*, 8272−8273.
44. Takamoto, K., He, Q., Morris, S., Chance, M. R., and Brenowitz, M. (2002) Monovalent cations mediate formation of native tertiary structure of the *Tetrahymena thermophila* ribozyme, *Nat. Struct. Biol. 9*, 928−933.
45. Perez-Salas, U. A., Rangan, P., Krueger, S., Briber, R. M., Thirumalai, D., and Woodson, S. A. (2004) Compaction of a bacterial group I ribozyme coincides with the assembly of core helices, *Biochemistry 43*, 1746−1753.
46. Takamoto, K., Das, R., He, Q., Doniach, S., Brenowitz, M., Herschlag, D., and Chance, M. R. (2004) Principles of RNA compaction: Insights from the equilibrium folding pathway of the P4−P6 RNA domain in monovalent cations, *J. Mol. Biol. 343*, 1195−1206.
47. Fang, X., Littrell, K., Yang, X. J., Henderson, S. J., Siefert, S., Thiyagarajan, P., Pan, T., and Sosnick, T. R. (2000) Mg^{2+}-dependent compaction and folding of yeast tRNAPhe and the catalytic domain of the *B. subtilis* RNase P RNA determined by small-angle X-ray scattering, *Biochemistry 39*, 11107−11113.
48. Chauhan, S., Caliskan, G., Briber, R. M., Perez-Salas, U., Rangan, P., Thirumalai, D., and Woodson, S. A. (2005) RNA tertiary interactions mediate native collapse of a bacterial group I ribozyme, *J. Mol. Biol. 353*, 1199−1209.
49. Russell, R., Das, R., Suh, H., Travers, K. J., Laederach, A., Engelhardt, M. A., and Herschlag, D. (2006) The paradoxical behavior of a highly structured misfolded intermediate in RNA folding, *J. Mol. Biol. 363*, 531−544.
50. Baird, N. J., Westhof, E., Qin, H., Pan, T., and Sosnick, T. R. (2005) Structure of a folding intermediate reveals the interplay between core and peripheral elements in RNA folding, *J. Mol. Biol. 352*, 712−722.
51. Misra, V. K., and Draper, D. E. (1999) The interpretation of Mg^{2+} binding isotherms for nucleic acids using Poisson-Boltzmann theory, *J. Mol. Biol. 294*, 1135−1147.
52. Ni, H., Anderson, C. F., and Record, M. T., Jr. (1999) Quantifying the thermodynamic consequences of cation (M^{2+}, M^{+}) accumulation and anion (X^{-}) exclusion in mixed salt solutions of polyanionic DNA using Monte Carlo and Poisson-Boltzmann calculations of ion-polyion preferential interaction coefficients, *J. Phys. Chem. B 103*, 3489−3504.
53. García-García, C., and Draper, D. E. (2003) Electrostatic Interactions in a Peptide-RNA Complex, *J. Mol. Biol. 331*, 75−88.
54. Misra, V. K., and Honig, B. (1995) On the magnitude of the electrostatic contribution to ligand-DNA interactions, *Proc. Natl. Acad. Sci. U.S.A. 92*, 4691−4695.
55. Xie, Z., Srividya, N., Sosnick, T. R., Pan, T., and Scherer, N. F. (2004) Single-molecule studies highlight conformational heterogeneity in the early folding steps of a large ribozyme, *Proc. Natl. Acad. Sci. U.S.A. 101*, 534−539.
56. Schimmel, P. R., and Redfield, A. G. (1980) Transfer RNA in Solution: Selected Topics, *Annu. Rev. Biophys. Bioeng. 9*, 181−221.

BI062284R